Section 1
PROGRESS IN LASER FUSION

1.A Interpretation of Recent Argon Experiments on OMEGA

Argon-filled polymer shell implosions are of interest because, unlike fuel-filled shells, they can be diagnosed using line-spectroscopy methods. In addition, the deceleration instability may be mitigated in these targets because of the high target-core density. Polymer shells have the important advantage over glass targets in that they attenuate argon lines to a much lesser extent. However, recent experiments have shown that the argon lines are very strongly absorbed by a cooler argon plasma surrounding the core. Therefore, the density diagnostics of the core are lost. However, we show here that the absorption can in turn be used to diagnose that cooler argon region. We also show that radiation at wavelengths away from absorption lines is little attenuated by the cooler argon, and it can yield information about the hot core, primarily its temperature.

Four regions in an imploded argon-filled CH shell are shown schematically in Fig. 49.1. The regions are (a) the hot central core, emitting a strong continuum, (b) a cooler argon region surrounding the core, where the absorption lines in partially ionized argon are formed; the helium-like and hydrogen-like argon lines emitted in region (a) are also strongly absorbed here, (c) the compressed, low-temperature part of the polymer shell, and (d) the ablated, laser-heated part of the polymer shell.

Hydrodynamic mixing between adjacent target regions may adversely affect target performance, and some evidence to that effect, in the existing data, will be described.

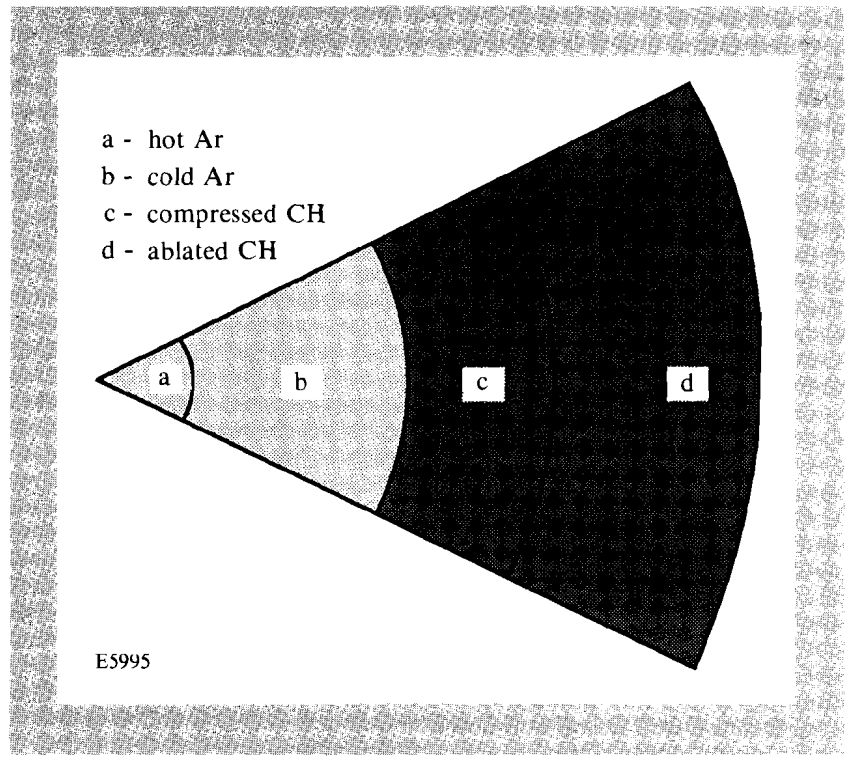

Fig. 49.1
Schematic representation of relevant regions in the argon-filled CH shell target. Argon lines emitted in region (a) are absorbed within region (b).

The data is from a series of shots taken as a part of NLUF experiments conducted by C. F. Hooper of the University of Florida (jointly with an LLE group) and reported in Ref. 1. In these experiments, argon-filled plastic shells of diameter 250 μm and thicknesses of 6, 8, 10, and 12 μm were imploded with 600-ps FWHM, 1200-J laser pulses. The targets were filled with 20 atm of argon and were coated with 0.05 μm of aluminum. The 24 OMEGA beams were smoothed by spectral dispersion[2] (SSD) at a frequency of 8.45 MHz with a bandwidth $\Delta\lambda/\lambda = 2.7 \times 10^{-4}$. The results are shown in Figs. 49.2 and 49.3. Figure 49.2 shows the time-integrated spectra for shots 20876, 20878, 20882, and 20886. The experimental parameters for these shots were similar, except for the shell thicknesses of 6, 8, 10, and 12 μm, respectively. Figure 49.3 shows the streaked spectrum for shot 20878 (8-μm thickness).

Absorption Lines in Argon Ions

The most striking feature in these figures is the absorption lines in the range 2.9–3.1 keV, formed within the continuum emitted by the hot target core. These lines are due to 1s–2p transitions in argon ions having n electrons ($n = 0$–7) in the L shell. They have been used in the past[3,4] to determine the $\rho\Delta r$ of the absorption region within the shell. Here, the absorption region is within the fill gas rather than the shell (the CH shell has no absorption lines because it is mostly stripped of electrons; even if it were not stripped, the strong photoionization absorption at the low-energy position of the carbon lines would wipe out any line-absorption features). The absorption in argon is strong enough to cause extinction, i.e., in the region of flat spectrum (around 3.05 keV) essentially all the core-emitted photons are absorbed on the way out. In that case, only a lower bound on the $\rho\Delta r$ of the absorption region can be obtained.

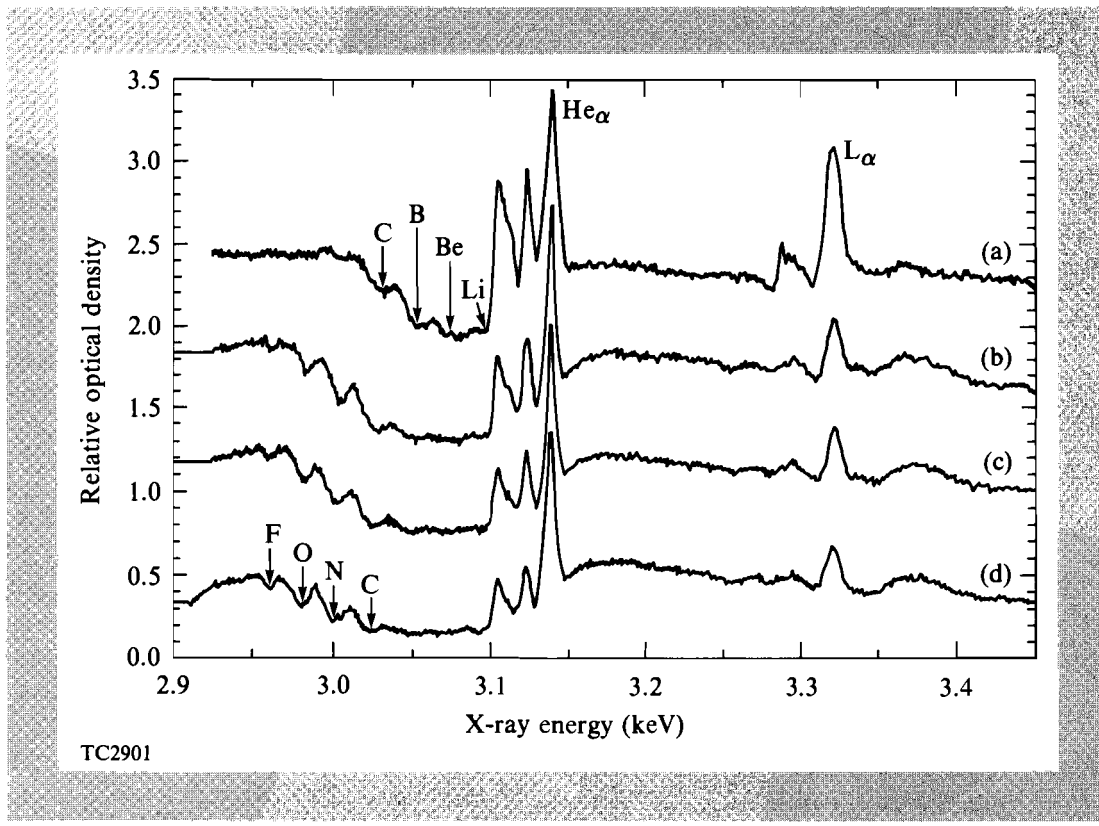

Fig. 49.2
Time-integrated spectra for shots 20876, 20878, 20882, and 20886. The experimental parameters for these shots were similar, except for shell thicknesses of 6, 8, 10, and 12 μm, respectively. The four spectra are shifted vertically for clarity. The zero (i.e., film background) level for these spectra is essentially that of the lowest density around 3.08 keV.

The temperature in the absorption region can only be estimated because of the extinction caused by strong line absorption. When the $\rho\Delta r$ of the absorbing layer is sufficiently small, the intensity contour of the group of absorbing lines is obtained, which yields the distribution of charge states, hence the temperature. In fact, a similar absorption manifold within a thin layer in the shell[4] had no extinction and enabled us to estimate the temperature in the cold part of the shell. A more precise determination of the temperature of the absorption layer in the present case may become possible with a lower argon fill pressure, which will reduce the absorption in these lines.

The progression to thicker shells in Fig. 49.2 [curves (a)–(d)] indicates an increasing $\rho\Delta r$ of the absorbing region [(b) in Fig. 49.1]. This is evidenced by the observation that at any wavelength, the emitted intensity goes down with increasing shell thickness, until extinction is reached. However, code simulations for these experiments have shown[1] that the total argon $\rho\Delta r$ should decrease with increasing shell thickness. This point should be further studied; it could be that because the temperature falls with increasing shell thickness, the total argon $\rho\Delta r$ decreases even as the $\rho\Delta r$ of the cold layer increases.

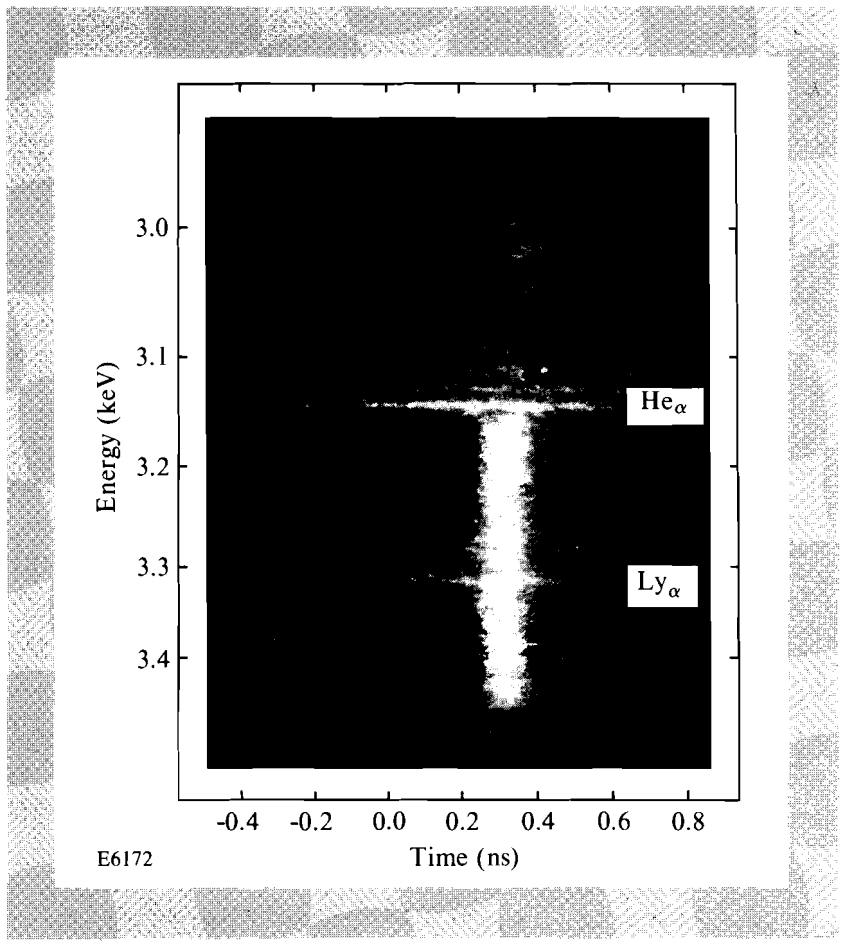

Fig. 49.3
Streaked spectrum for shot 20878 (CH shell of 8-μm thickness). The time scale zero is arbitrary. The narrow argon lines are emitted by the argon enclosed within the polymer shell. Around peak compression, a strong continuum is emitted at energies higher than about 3.15 keV; absorption by argon ions cuts its intensity at lower photon energies.

We next estimate a lower bound on the $\rho\Delta r$ of the argon absorption layer, using the equation[4]

$$\rho\Delta r = \frac{m c M_i}{f \pi e^2 \alpha} \int \ln \frac{I_o}{I_\nu} d\nu \, . \tag{1}$$

Here M_i is the ionic mass, α is the fraction of the ions in the ground state, I_o is the unabsorbed intensity level (read outside the spectral region of absorption lines at, say, 2.95 keV), and the integral is over the intensity I_ν of each absorption line. The absorption oscillator strength f has to be averaged over the lower-state levels as well as summed over the upper-level states (of which there can be a few tens,[4] within each absorption line in Fig. 49.2). Equation (1) gives the $\rho\Delta r$ of one ionic species, using a single absorption line in Fig. 49.2; the total $\rho\Delta r$ is obtained by summing the (deconvolved) contributions from all the observed absorption lines. For lines showing extinction (i.e., a flat intensity level) a lower bound on the corresponding $\rho\Delta r$ is obtained by assuming that they just broaden enough to merge with their neighboring lines. Using this procedure we estimate $\rho\Delta r \geq 3.2$ mg/cm^2. Two correction factors need to be applied, one is a finite-temperature correction[5] and the other a fluorescence correction.[6] Both corrections increase the estimated $\rho\Delta r$ and the corrected estimate becomes $\rho\Delta r \geq 5$ mg/cm^2.

To compare this estimate with the simulation results, we show in Fig. 49.4 the predicted temperature and density profiles for shot 20886 [spectrum (d) in Fig. 49.2]. The range of temperatures $T \leq 500$ eV is consistent with the ionization of argon ions up to the He-like charge state; thus, this is where the absorption lines of Fig. 49.2 would be formed. According to Fig. 49.4 the absorbing region extends from a radius of 15 μm outwards, and its $N_e\Delta r$ value is $\sim 1 \times 10^{21}$ cm^{-2}. For an average ionization of $Z = 14$ (B-like argon), this corresponds to $\rho\Delta r = 4.7$ mg/cm^2, in good agreement with the value estimated from the experiment. A detailed atomic-population calculation should improve the precision of the predicted $\rho\Delta r$.

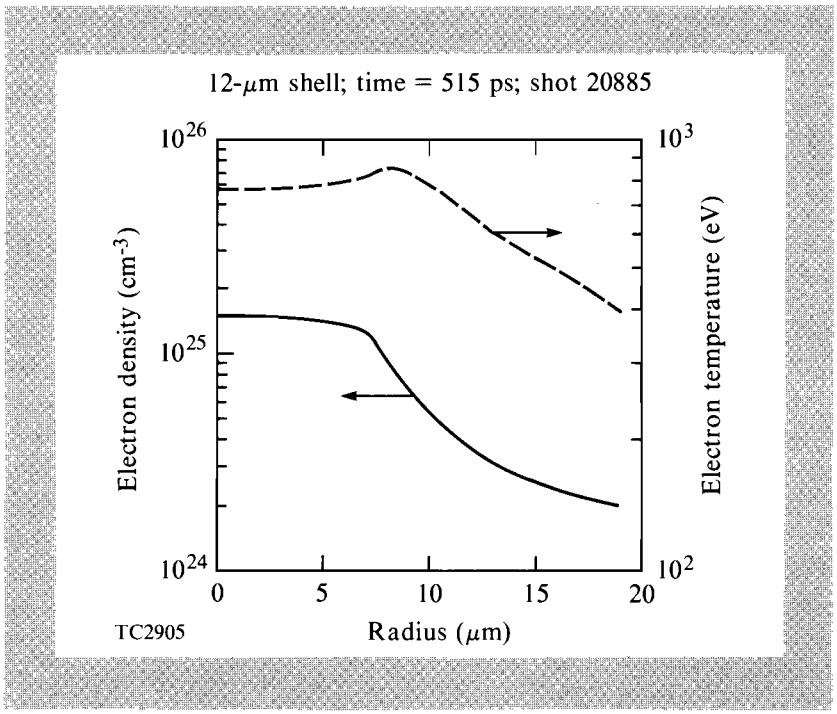

Fig. 49.4
The predicted temperature and density profiles for shot 20886 [spectrum (d) in Fig. 49.2]. The temperature gradient gives rise to the layer classification of Fig. 49.1.

An additional interesting feature related to the absorption lines is seen in the time-resolved data of Fig. 49.3. Around the time of peak compression there is a strong flare-up of continuum radiation at energies above the He_α line, caused by an increase in both the temperature and the density of the argon core. The absorption lines of Fig. 49.2 are seen in Fig. 49.3 for a brief period of time following peak compression (defined as the time of maximum continuum intensity). Obviously, when the continuum decays because of target expansion and cooling, the absorption lines should also disappear. However, Fig. 49.3 shows their appearance lags behind the onset of rise in the continuum intensity. When the continuum is already intense but the absorption lines have not yet appeared, the absorption is sufficiently high to cause extinction of all radiation, even at wavelengths between the absorption lines. As a comparison, Fig. 49.5 shows two predicted time-resolved spectra in the spectral range where the absorption lines appear. The figure shows that indeed the absorption lines should appear only after a complete extinction at the time of peak compression. The time difference between the two spectra in Fig. 49.5 is 38 ps; this is consistent with

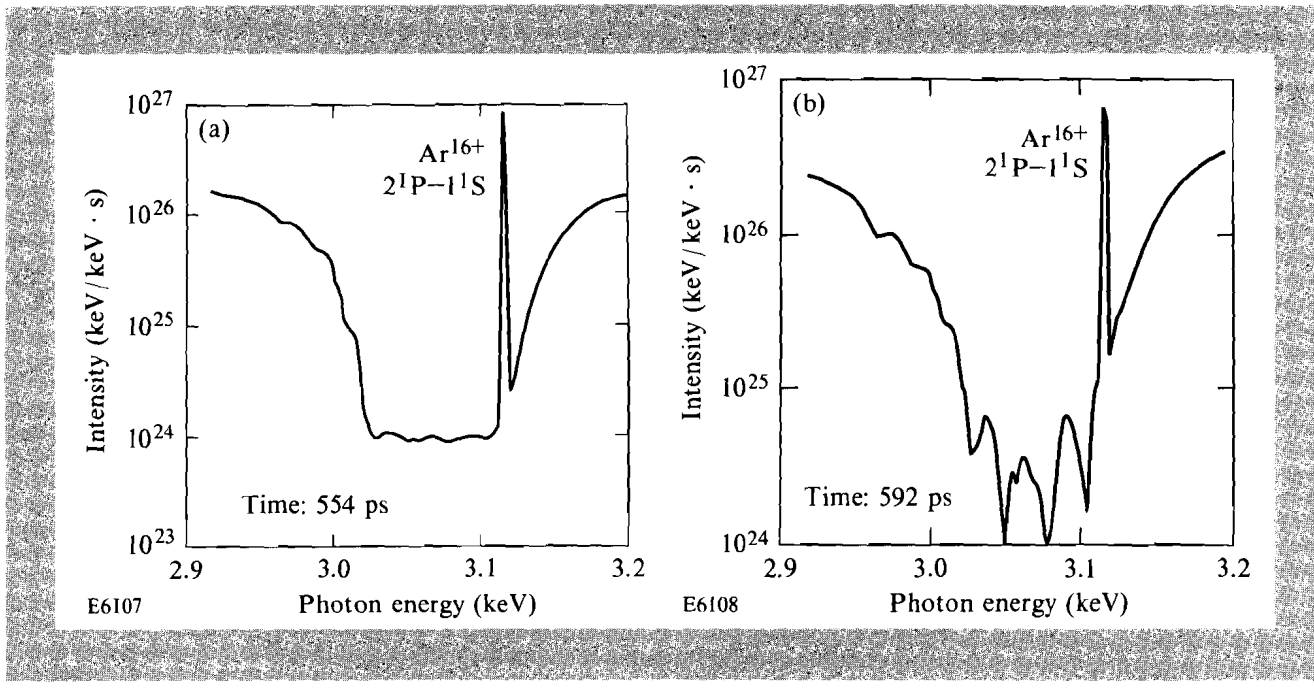

Fig. 49.5
The *LILAC*-predicted time-resolved spectra, in the spectral range where the absorption lines appear: (a) at the time 554 ps after the peak of the pulse, and (b) 38 ps later. Good agreement is seen with the experimental data of Fig. 49.3: complete absorption in the spectral range 3.0–3.1 keV, followed by the appearance of absorption lines.

Fig. 49.3, where the time of complete extinction precedes the time of absorption-line appearance by $\lesssim$ 80 ps. A close examination of the code results shows that this decrease in absorption is caused by the shock reflection at the target center. When the converging shock reaches the center [about the time of Fig. 49.5(a)], the hot central core becomes surrounded by a cooler, absorbing argon. However, at the time of Fig. 49.5(b), the reflected shock reaches the peripheral argon layer and heats it, thereby reducing its absorptivity.

Helium-like and Hydrogen-like Argon Lines

The lines of helium-like and hydrogen-like argon, unlike the lines studied in the preceding section, can appear in absorption as well as in emission. Thus, these lines represent a special case. They are emitted in plasma regions where the temperature is high enough for the excitation by electron collisions of 1s–2p transitions, which leads to 2p–1s spontaneous line emission. On the other hand, the ions with some electrons in the *L*-shell (Li-like and lower ionizations) exist in low-enough temperature regions, where electrons cannot excite 1s–2p transitions. However, the continuum radiation from the hot core can excite these transitions, thus forming the observed absorption lines. The resulting emission following such excitation (or fluorescence) merely causes a small reduction in the depth of the absorption features.[6]

The diagnosis based on helium-like and hydrogen-like argon lines is further complicated by the existence of argon in the CH shell. In fact, the strong and narrow emission argon lines in Figs. 49.2 and 49.3 are deemed to be emitted

mainly by the argon in the polymer shell, rather than by the argon fill gas. This conclusion follows from the observation in Fig. 49.3 that the intensity of these lines peaks earlier than peak compression, and that even for a modest compression they would have been much broader (see the following) if originating from the argon fill gas. If the argon emission lines in Figs. 49.2 and 49.3 are indeed emitted primarily in the shell, then subtracting them out leads to the conclusion that the argon lines emitted by the core are absorbed by the cooler argon layer [region (b) in Fig. 49.1], thus do not emanate from the target. This is indeed the predicted behavior, as seen in Fig. 49.6, showing the calculated spectrum around peak compression for the 12-μm-thick shell implosion. Argon fill gas was assumed to uniformly fill the shell, including the wall. The argon in the wall gives rise to emission lines, which appear very narrow because of the lower $\rho\Delta r$ in the shell. These narrow lines are superimposed on Stark-broadened argon lines that appear in absorption, because even the continuum at the wavelengths of the argon lines is absorbed by the cooler argon layer. The predicted (Fig. 49.6) and measured (Fig. 49.2) argon lines compare quite well, especially when we allow for the instrumental broadening of the argon lines from the shell, which was not included in the simulation of Fig. 49.6. In particular, curve (d) in Fig. 49.2 shows what appears to be the high-energy wing of an absorbed He_α line (around 3.15 keV). This is an indication of broad absorption profiles of argon resonance lines, which are masked by the emission of narrow lines from the argon in the shell; this is particularly the case for the He_α line.

A more conclusive measurement will be attempted with the He_β line at 3.68 keV, which was outside the range of the spectra in Figs. 49.2 and 49.3. As Fig. 49.6 shows, the Stark broadening of this line is much larger. Measuring this

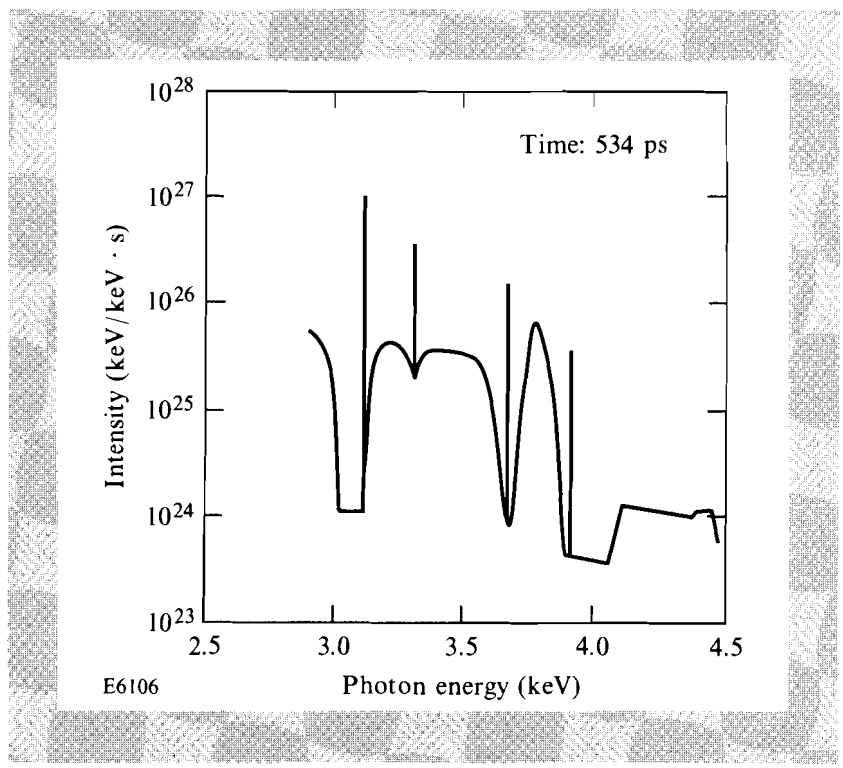

Fig. 49.6
The calculated spectrum around peak compression for the 12-μm-thick shell implosion. Argon fill gas was assumed to uniformly fill the shell, including the wall. The code correctly replicates the absorption in the spectral range 3.0–3.1 keV (see Fig. 49.2) as well as the narrow line emission caused by argon trapped within the polymer shell.

line profile could have demonstrated the existence of two distinct line-profile components: narrow emission line coming from the shell, and a broad profile formed in the cooler argon layer. The density in the absorption region can then be directly determined from the absorption Stark profile.

It is interesting to compare the results discussed here with an earlier experimental series where argon-filled polymer shells were also used.[7] In that series, bigger and thinner shells were imploded with a higher-energy laser, which was not smoothed by spectral dispersion (but DPP's were employed). Typically, shells of diameter 420 μm and thickness 6 μm were filled with 10-atm argon fill pressure and imploded with 1700-J laser pulses of 680-ps FWHM. An overcoat layer of 0.05-μm Al was also applied to the targets. There is a striking difference between the results in that series and those of Fig. 49.3. There (Fig. 2 of Ref. 7), strong and broad argon lines appear in emission, whereas such lines are missing completely in Fig. 49.3. In the code-calculated spectrum for the conditions of Ref. 7, the He_α line is predicted to be totally absorbed (except for a narrow-line emission from the shell). This striking disagreement with the code may be because of mixing of target layers (a) and (b) (Fig. 49.1) in that earlier series of experiments. To observe absorption lines, the hot core should be totally surrounded by the cooler layer, and mixing of the two layers enables the inner radiation to escape with little absorption. On the other hand, both the He_α and the Ly_α core-emitted lines in Figs. 49.2 and 49.3 agree with the predictions of Fig. 49.6, after subtracting out the narrow lines caused by the argon in the shell: both appear in absorption.

Argon Core Continuum Emission and Absorption

In addition to the spectral-line diagnosis described previously, the continuum emission and absorption can also be a source of information. The continuum emitted by the hot argon core [region (a) in Fig. 49.1] can be absorbed on its way out, primarily in region (b). Absorption on 1s–2p transitions leading to the appearance of absorption lines in the spectrum was dealt with previously. Here we turn to continuum absorption, primarily caused by the photoelectric effect.

The total continuum absorption in cold argon in the range 2.8–3.5 keV is shown in Fig. 49.7. Below the *K*-edge at 3.2 keV the continuum absorption is insignificant in comparison with the line absorption in the same spectral region. However, there is no line absorption below the F-like absorption peak around 2.96 keV, because for Ne-like and lower ionizations, no 1s–2p transition into the full *L*-shell is possible. Because of the rise in continuum bound-free absorption towards lower photon energies (like ν^{-3}), at some point below 2.95 keV the absorption in the cool argon layer will be strong enough to cause the observed continuum (emitted by the hot argon core) to start declining. In Fig. 49.2 it appears as if that indeed is the case for the 12 μm shell. However, because of overlap of spectra caused by reflection from different crystal planes, no firm conclusion can be drawn. We can estimate the expected attenuation at 2.9 keV, within the cool argon layer, based on the $\rho\Delta r$ for that layer, as estimated previously. The opacity of cold argon at 2.9 keV is 190 cm^2/g. Since the *L*-shell of ions in the absorption layer is on the average half empty (the sequence of species corresponding to the absorption lines in Fig. 49.2 have

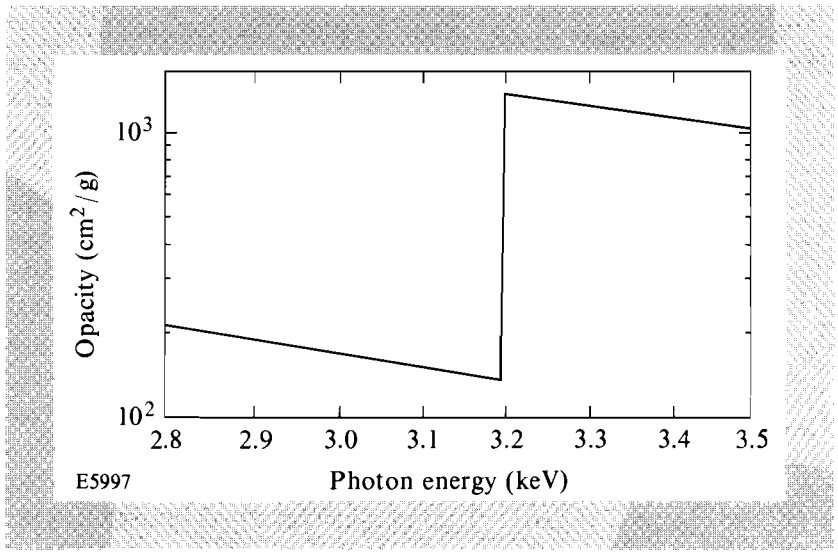

Fig. 49.7
The total continuum absorption in cold argon in the range 2.8–3.5 keV. The strong continuum observed above 3.2 keV (Fig. 49.3) is because of the ionization of the argon in region (b) of Fig. 49.1.

from 2 to 7 electrons in the *L*-shell). Thus, the opacity at 2.9 keV is ~95 cm^2/g, and the $\rho\Delta r$ of 5 mg/cm^2 gives an attenuation by a factor of $\exp(-0.47) = 0.6$.

Above the *K*-edge, the opacity of cold argon increases abruptly (Fig. 49.7) but the core-emitted continuum is nevertheless very intense (see Fig. 49.3). This indicates that very little of the argon in the cool layer is cool enough to be neutral. To further explain this, we start by determining the positions of the *K*-edges for argon ions. Since they are not tabulated in the literature, we rely on published[8] K_α line energies in ionized argon. As an example, the method of determining the *K*-edge energies is shown schematically in Fig. 49.8 for the Be-like argon ion. The energy difference between the states (A) and (B) is just the tabulated[8] K_α line energy for Li-like argon; the energy difference between states (B) and (C) is the tabulated[9] ionization energy of Be-like argon. Thus, by adding the two we obtain the energy difference between (A) and (C), i.e., the *K*-edge energy for Be-like

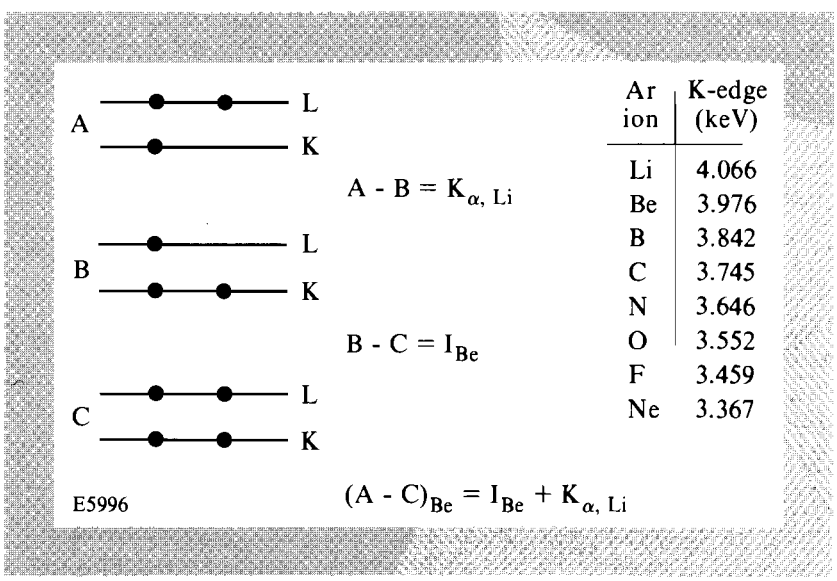

Ar ion	K-edge (keV)
Li	4.066
Be	3.976
B	3.842
C	3.745
N	3.646
O	3.552
F	3.459
Ne	3.367

Fig. 49.8
Schematic representation of the method of determining the *K*-edge energies of argon ions (here, the Be-like argon).

argon. The tabulated results in Fig. 49.8 show that for all the argon ions known to exist in the absorbing layer (i.e., F-like and higher ionizations), the corresponding K-edges fall outside the spectral range of Fig. 49.2. Thus, if no lower ionizations than F-like exist in the shell (which would be true if the shell temperature is at no place lower than ~50 eV), no K-shell photoionization absorption will occur in the spectral range of Fig. 49.2. Extending the measurement to higher photon energies than those of Fig. 49.2 may not reveal the absorption edges corresponding to these K-edges either. This is because the absorption is divided among the various argon-ionic species, each having an edge at a different spectral location. The opacity above the cold K-edge (Fig. 49.7) is ~10^3 cm^2/g, which for a $\rho\Delta r$ of 5 mg/cm^2 would yield an attenuation by a factor exp(−5); however, divided among, say, 10 species, the attenuation at any edge will only be about exp(−0.5). It should be noted that the increase in continuum intensity near 3.35 keV is instrumental and is caused by an increase in film sensitivity (the LIII edge of silver is at 3.35 keV).

Based on the previous conclusion that target region (b) (in Fig. 49.1) is quasi-transparent to the continuum for energies above ~3.15 keV, the temperature of the hot argon core can be determined through the slope of the observed continuum emission in that spectral region. Figure 49.2 indicates that the temperature falls for increasing shell thickness, as predicted; however, a more quantitative temperature determination should await the overcoming of the crystal reflection overlap problem. Coupled with this temperature determination, the relative intensity of the continuum can be used to estimate the change in the ρr of the hot argon core region, for increasing shell thickness.

In conclusion, the diagnosis (with argon spectroscopy) of compressed targets having core-temperature gradients requires special care. In the case of high fill pressure of argon (several atmospheres), the argon lines will appear in absorption and yield information on the conditions (primarily the density and the $\rho\Delta r$) of the peripheral argon layer. On the other hand, the continuum radiation can yield information on the conditions (primarily the temperature) of the central argon core. For an argon fuel mixture where the argon constitutes a sufficiently small fraction, the argon lines will appear in emission and provide diagnostics information on the conditions of the central core.

ACKNOWLEDGMENT

This work was supported by the U.S. Department of Energy Office of Inertial Confinement Fusion under agreement No. DE-FC03-85DP40200 and by the Laser Fusion Feasibility Project at the Laboratory for Laser Energetics, which is sponsored by the New York State Energy Research and Development Authority and the University of Rochester.

REFERENCES

1. J. Delettrez, R. Epstein, D. K. Bradley, P. A. Jaanimagi, R. C. Mancini, and C. F. Hooper, Jr., "Hydrodynamic Simulation of Non-LTE Atomic Physics of High-Density Implosions of Ar-filled Polymer Shell Targets," in the *Proceedings of the International Workshop on Radiative Properties of Hot Dense Matter*, Sarasota, FL, 22–26 October 1990.
2. S. Skupsky, R. W. Short, T. Kessler, R. S. Craxton, S. Letzring, and J. M. Soures, J. Appl. Phys. **66**, 3456 (1989).